This article has been accepted for publication in a future issue of this journal, but has not been fully edited. Content may change prior to final publication. Citation information: DOI 10.1109/TII.2017.2651146, IEEE Transactions on Industrial Informatics



# Multi-period Risk-limiting Dispatch in Power Systems with Renewables Integration

Chaoyi Peng, *Student Member*, *IEEE*, Yunhe Hou, *Senior Member*, *IEEE*, Nanpeng Yu, *Senior Member*, *IEEE*, Jie Yan, Shunbo Lei, and Weisheng Wang, *Senior Member*, *IEEE*

***Abstract*—In this paper, an improved multi-period risk-limiting dispatch (IMRLD) is proposed as an operational method in power systems with high percentage renewables integration. The basic risk-limiting dispatch (BRLD) is chosen as an operational paradigm to address the uncertainty of renewables in this paper due to its three good features. In this paper, the BRLD is extended to the IMRLD so that it satisfies the fundamental operational requirements in the power industry. In order to solve the IMRLD problem, the convexity of the IMRLD is verified. A theorem is stated and proved to transform the IMRLD into a piece-wise linear optimization problem which can be efficiently solved. In addition, the locational marginal price of the IMRLD is derived to analyze the effect of renewables integration on the marginal operational cost. Finally, two numerical tests are conducted to validate the IMRLD.**

***Index Terms*—Multi-period, operational requirements, risk-limiting dispatch, renewables integration, risk metric.**

## I. Introduction

THE global warming and the energy crisis are the most critical issues in this century. Renewable energy is flourishing these years as one of the most effective ways to reduce fossil fuel consumption. Total installed capacity of renewable energy resources keeps increasing in the past decade.

The intermittency and uncertainty from renewable energy resources bring many challenges to power system operation. Stochastic programming (SP) is adopted to address the uncertainty in the power system operation in many studies, such as the scenario-based two-stage unit commitment [1], and the model predictive control based look-ahead dispatch [2].

Among the system operational methods using SP, the BRLD is one of the flagships due to three good features [3, 4]. First, the BRLD considers the chance of recourse decisions, so the operational decisions are adaptable to the latest forecast information of renewables. Second, operational risks are concerned and limited through multiple dispatch stages, so the BRLD naturally conforms to the industrial requirement on the risk assessment of renewables integration [5]. At last, the BRLD is able to render a global optimal operational decision, taking advantages of the conditional prediction of the uncertainty [3].

Despite the three advantages, the BRLD achieves the global optimal decision while sacrificing some fundamental industrial requirements. First, the BRLD assumes a single delivery period in an electricity market, but the real-time operation in the electricity market should be multi-period. For example, the delivery horizon of the day-ahead market is composed of 24 1-hour intervals in the Pennsylvania—New Jersey—Maryland (PJM) market [6]. Second, key power system operational constraints such as the inter-temporal unit ramping constraint and the transmission thermal limit constraint are missing in [3]. However, these constraints represent the basic physical features of power systems and the violation of them may lead to destructive consequences [7], [8]. Third, [3] uses a simplified risk metric in the form of probability. In the power industry and academic field, it is well acknowledged that a variety of alternative risk metrics are indispensable in quantifying the operational risk in appropriate situations [5]. These risk metrics include loss of load probability, loss of load frequency [9], value-at-risk [10] and conditional value-at-risk [11].

Due to these fundamental requirements on the system operation in the realistic power industry, the BRLD was extended in many ways. The operational framework of the BRLD was extended to include multiple delivery periods in [12] with closed form solutions based on dynamic programming. However, it is hard to integrate transmission networks and other risk metrics, in virtue of the combinational explosion of dynamic programming. Akin to [12], ramping capacity and energy storage were considered in the BRLD in [13], [14]. The effect of transmission network was considered in [15], where only one congested line existed in the network. However, this assumption is not tenable in realistic systems in which line congestions are one of the dominant factors preventing high percentage penetration of renewables [16]. [18] used a

This work was supported by the Theme-based Research Scheme through Project No. T23-701/14-N, National Science Foundation (NSF) under award #1637258, National Natural Science Foundation of China under Grant 51277155, Research Grant Council of Hong Kong SRA under Grants ECS739713 and GRF17202714, and Research funding from State Grid Corporation of China (SGLNSY00FZJS1601337).

Chaoyi Peng, Yunhe Hou and Shunbo Lei are with the Department of Electrical and Electronic Engineering, the University of Hong Kong, and HKU Shenzhen Institute of Research and Innovation, Shenzhen, China. (pcy1990@eee.hku.hk), (yhhou@eee.hku.hk), (leishunbo@eee.hku.hk)

Nanpeng Yu is with the Department of Electrical and Computer Engineering, University of California, Riverside (nyu@ece.ucr.edu)

Jie Yan is with the Economic Study Group, MISO (jyan@misoenergy.org)

Weisheng Wang is with the Renewable Energy Department, China Electric Power Research Institute (wangws@epri.sgcc.com.cn)

This article has been accepted for publication in a future issue of this journal, but has not been fully edited. Content may change prior to final publication. Citation information: DOI 10.1109/TII.2017.2651146, IEEE Transactions on Industrial Informatics



numerical method to solve the BRLD considering the transmission network and the ramping capacity under the framework of two-stage stochastic optimization, so the recourse decision cannot be taken into consideration, which leads to the sub-optimality of the operational strategies. Risk metrics other than LOLP were considered in [17], but the impact of the multi-period and the transmission network were not regarded. Lastly, none of the above works derived the locational marginal price for the operational model, so the sensitivity of loads and renewable injections to the operational cost was not provided therein, and the shadow prices of the load and renewables injection were not revealed.

Therefore, the knowledge gap of the existent studies is their insufficiency in satisfying the realistic operational requirements simultaneously. This paper extends the BRLD to the IMRLD to address this issue. Specifically, we model the IMRLD as a multi-stage multi-period operational problem. The unit ramping constraint and the transmission network constraint are incorporated, and the quantile and the superquantile are wielded as the risk metrics. To solve the IMRLD, we encounter two technical challenges. The first is the global optimality of the IMRLD, and the second lies in solving an optimization problem with a set of superquantile constraints. We prove the global optimality of the IMRLD by verifying its convexity, and we prove a theorem mathematically so that the optimization problem with a set of superquantile constraints can be equivalently transformed into a piece-wise linear optimization problem, which can be solved by existing solvers efficiently. In order to analyze the IMRLD, we derive the locational marginal price (LMP) to show the impact of renewables integration on system marginal operational costs.

In sum, the contributions of the paper can be summarized as follows:

(1) In terms of problem formulation, this paper extends the BRLD to the IMRLD which caters to the industrial requirements while preserves the good features of the BRLD.

(2) In terms of problem solving, this paper verifies the convexity of the IMRLD problem, and proves a theorem mathematically to transform the insolvable IMRLD into a conventional piece-wise linear optimization problem.

(3) In terms of problem analysis, this paper derives the analytic form of the locational marginal price to show the marginal operational cost related to loads and renewable injections for the IMRLD.

The remainder of the paper is organized as follows. Section II presents the IMRLD model. Section III solves the IMRLD by verifying the convexity and proving a theorem. The LMP is derived in Section IV. Section V applies the proposed IMRLD to a modified IEEE standard case and a realistic Gansu provincial power system in China. The final conclusions are given in Section VI.

## II. Model Formulation of the IMRLD

### A. Framework of the IMRLD

The basic idea of the IMRLD on multiple delivery periods is illustrated in Fig. 1.

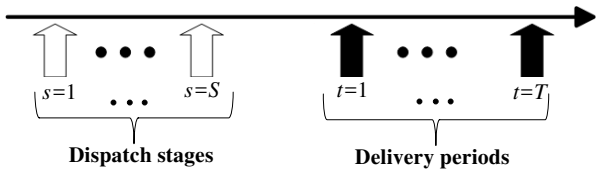


Fig. 1. The structure of the IMRLD.

We assume that the operational framework is composed of $T$ delivery periods (black arrows in Fig. 1) and $S$ dispatch stages (white arrows in Fig. 1). The $T$ delivery periods can be treated as real-time markets. The $S$ dispatch stages represent the dispatch processes in the day-ahead market and the intra-day market. The power in each delivery period is accumulated from dispatch stages (day-ahead and intraday) and that delivery period (real-time). In order to mitigate the operational risk, such as the risk of power unbalance and transmission line overload in each delivery period, the Independent System Operator (ISO) purchases power by signing contracts in all dispatch stages in the most economical way.

The general model of the IMRLD is formulated as (1)-(3):

$$\min E\sum_{t=1}^{T}\sum_{s=1}^{S} f_{st}(\mathbf{x}_{st}(Y_s, Y_{s+1}|Y_s,...,Y_S|Y_s), \mathbf{y}_{st}) \quad (1)$$

$$R_t(\mathbf{x}_{st}(Y_s, Y_{s+1}|Y_s,...,Y_S|Y_s), \mathbf{y}_{st}) \le Risk_t \quad (2)$$

$$\mathbf{x}_{st}(Y_s, Y_{s+1}|Y_s,...,Y_S|Y_s) \in \Omega,\ \mathbf{y}_{st} \in \Lambda \quad (3)$$

where $s$ and $t$ are the index of the stage and period respectively. The objective function $f_{st}(\cdot)$ represents the expected operational cost. $R_t(\cdot)$ is the risk function with an upper bound $Risk_t$. This risk function can take any risk metric for any given operational constraint. $Y_s$ is the prediction information at stage $s$. $\mathbf{y}_{st}$ is the vector of state variables, such as the power flow and the phase angle, belonging to a feasible region $\Lambda$. Each decision vector $\mathbf{x}_{st}$, belonging to another feasible region $\Omega$, denotes the power purchased at dispatch stage $s$ for delivery period $t$, as a function of the conditional predictions ($Y_s$, $Y_{s+1}|Y_s$,…, $Y_S|Y_s$).

The dispatch process is illustrated in Fig. 2.

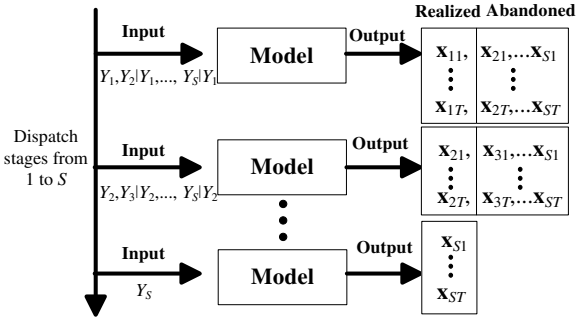


Fig. 2. Operational process.

Dispatch stages: in dispatch stage 1, ISO solves (1)-(3) to obtain the power to be purchased from stage 1 to stage $S$ with the input ($Y_1$, $Y_2|Y_1$,…, $Y_S|Y_1$.). Only $\mathbf{x}_1$ is enforced whereas the rest dispatch outputs are advisory. When times rolls forward, the prediction information will be updated, and the above calculation repeats again and again until the last dispatch stage $S$. By the end of the dispatch stages, the power accumulated for each delivery stage $t$ is $\sum_i \mathbf{x}_{it}$.

Delivery periods: wind power generation may be different from the forecast due to the uncertainty. If the power

This article has been accepted for publication in a future issue of this journal, but has not been fully edited. Content may change prior to final publication. Citation information: DOI 10.1109/TII.2017.2651146, IEEE Transactions on Industrial Informatics



accumulated from previous dispatch stages cannot balance the load at one delivery period, the power shortage should be compensated from the corresponding real-time markets. Furthermore, if there is still a power shortage or the thermal limits of transmission lines are violated, compulsory load shedding is inevitable. Therefore, the power is a sum of the cumulated power from all dispatch stages for each delivery period, the power from the real-time market, and the negative power consumption resulting from load shedding, if necessary.

According to the Bellman optimality principle, the solution process of the IMRLD can be decoupled into $(S+T)^{\text{th}}$ optimization problems. Therefore, the IMRLD is solved $(S+T)^{\text{th}}$ times to achieve the final global optimal decision [3]. The general model of the IMRLD is specified in the following subsections.

### B. Simplifying assumption

The following simplifying assumptions are made in our model.

(1) We assume that market participants are price-takers. This assumption is acceptable if quantities of the power to be traded are large in the market [19]. This assumption has been widely used in many textbooks [19-20], technical reports [21] and research papers [22], because it brings a decentralized market solution process [20]. The situation where the wind power serves as a price-maker is out of scope of this paper [23].

(2) The operational constraints are grouped into two categories due to the uncertainty of renewables. The first type of constraints are considered as soft constraints, of which the violating probability and potential losses should be assessed by risk metrics. Transmission line overload is treated as the soft constraint in this paper, because utilities concern the severity of transmission line overload, e.g. costs associated with the overload, in addition to its probability. For example, Midcontinent Independent System Operators uses Transmission Constraint Demand Curves to quantify the severity of overload by penalty prices [24]. North American Electric Reliability Corporation (NERC) uses different short term ratings for transmission lines to distinguish severity levels of system failures [25]. In addition, quite a few research works also used operating risk to assess the transmission line overload [26], [27]. In this regard, the transmission line overload is defined as the soft constraint in this paper. The second type constraint is considered as a hard constraint which must be satisfied at all times. The real power balance and the unit max/min capacity constraint are good examples of the hard constraint.

(3) Electricity demands are modeled as inelastic loads, so the objective function of the system operation is the minimization of total dispatch cost rather than the maximizing of social surplus. However, price-sensitive demand bids can be easily integrated into the proposed framework.

(4) The model is based on the DC power flow. This assumption is tenable for high voltage and long distance transmission networks, where DC power flow is a good approximation of the AC power flow for system steady state operation [28]. In this sense, DC power flow is used both in the industrial and academic field in transmission-level system operation [29], [30].

### C. Risk metrics

Based on the above assumptions, the operational risk of violating the thermal limit depends on the choice of risk metrics, which is the risk function $R_{st}(\cdot)$ in (2). In engineering field, the commonly used risk metrics are expectation, worst case, quantile, safety margin, and superquantile [31]. This paper chooses the quantile and the superquantile as a paradigm to measure the risk. Reasons for such choice are given as follows.

Of these five risk metrics, the expectation is simple but does not reflect the risk averseness of operators. The worst-case is conservative and uses no information of the probability distribution other than its highest realization. The safety margin may not detect large variation on the tail loss, which is important to operators. However, the quantile and the superquantile, also known as value at risk (VaR) and conditional value at risk (CVaR) in finance, take advantages of the probability distribution and the risk preference of operators can be tuned. The quantile has been identified as a risk metric when dealing with uncertainties in power systems by NERC [4]. Meanwhile, the superquantile is widely used as a risk measure in both industrial and academic field [32], because it has some good properties in the model formulation and solution. First, it meets the requirement of system operators on quantifying the uncertainty with a low probability but a high consequence. Second, it is a coherent and convex risk metric, so a global optimal decision can be achieved, which is desirable for system operators. It should be noted that the choice of risk metrics could be replaced by other metrics without affecting the whole methodology.

**Quantile**. Given a random variable $Z$ and its cumulative distribution function (CDF) $F_Z$, the $\alpha$-quantile is:

$$q_\alpha(Z) = F_Z^{-1}(\alpha) \tag{4}$$

Similarly, if the loss is a function of $Z$, denoted as $f(Z)$, then the risk of loss is determined by $q_\alpha(f(Z))$. Mathematically, this is equal to the failure probability $p(f(Z))$, where $p(f(Z))=\text{prob}(f(Z)>0)$, because of:

$$p[f(Z)] \le 1-\alpha \text{ iff } q_\alpha[f(Z)] \le 0 \tag{5}$$

**Superquantile**. Similarly, given the loss function, the $\alpha$-superquantile is:

$$\bar{q}_\alpha[f(Z)] = \frac{1}{1-\alpha}\int_{f(Z)\ge q_\alpha(Z)} f(Z)\,p(Z)\,dZ \tag{6}$$

In spite of its complex form, the superquantile is a coherent and convex metric [31], so it is widely used in both financial and engineering fields.

Based on these risk metrics, the risk constraint (2) is specified as the quantile constraint and the superquantile constraint, so the IMRLD to be solved has two versions, which are the IMRLD with the quantile constraint and the IMRLD with the superquantile constraint.

### D. IMRLD model with the quantile constraint

For the general model of the IMRLD in (1)-(3), we first use the quantile as the risk metric of the IMRLD, shown in (7)-(13).

This article has been accepted for publication in a future issue of this journal, but has not been fully edited. Content may change prior to final publication. Citation information: DOI 10.1109/TII.2017.2651146, IEEE Transactions on Industrial Informatics



At each dispatch stage *s*, the objective function (1) can be specified as:

$$\min E[\sum_{t=1}^{T}\sum_{s=1}^{S}(\mathbf{c}_{st}\mathbf{p}_{st})+\sum_{t=1}^{T}(\mathbf{m}_{\mathrm{l}t}\mathbf{r}_{\mathrm{l}t}+\mathbf{m}_{\mathrm{w}t}\mathbf{r}_{\mathrm{w}t})] \quad (7)$$

which minimizes the expected total operational cost for the whole delivery period. Decision variables are $\mathbf{p}_{st}$, $\mathbf{r}_{\mathrm{l}t}$ and $\mathbf{r}_{\mathrm{w}t}$, where $\mathbf{p}_{st}$ is the power output vector for each bus at dispatch stage *s* for delivery period *t*, $\mathbf{r}_{\mathrm{l}t}$ and $\mathbf{r}_{\mathrm{w}t}$ are the load shedding and wind spillage. The operational price $\mathbf{c}_{st}$, the load shedding price $\mathbf{m}_{\mathrm{l}t}$ and the wind spillage price $\mathbf{m}_{\mathrm{w}t}$ are constants in (7).

The constraint (3) of the decision variables is the hard constraint without risk. They are transformed to (8)-(11) as:

$$\sum_{s=1}^{S}\mathbf{p}_{st}+\mathbf{w}_t+\mathbf{r}_{\mathrm{l}t}-\mathbf{d}_t-\mathbf{r}_{\mathrm{w}t}=\mathbf{B}\boldsymbol{\theta}_t \quad \forall t \quad (8)$$

$$\mathbf{P}_{\min}\le\sum_{s=1}^{S}\mathbf{p}_{st}\le\mathbf{P}_{\max}, \quad \forall t \quad (9)$$

$$\mathbf{P}^{\mathrm{D}}\le\sum_{s=1}^{S}\mathbf{p}_{st}-\sum_{s=1}^{S}\mathbf{p}_{st-1}\le\mathbf{P}^{\mathrm{U}}, \quad \forall t \quad (10)$$

$$\mathbf{P}_{\min}\le\mathbf{p}_{st}\le\mathbf{P}_{\max}, \qquad \forall t,\forall s \quad (11)$$

where random variable $\mathbf{w}_t$ is the wind power vector predicted for delivery period *t*, and $\mathbf{d}_t$ is the demand at period *t*. Constants are the lower and upper bounds of the generation output limits $\mathbf{P}_{\min}$ and $\mathbf{P}_{\max}$, the lower and upper bounds of the ramping capabilities $\mathbf{P}^{\mathrm{D}}$ and $\mathbf{P}^{\mathrm{U}}$, and the B-matrix of the DC power flow **B**. (8) is the nodal power balance equation and $\boldsymbol{\theta}_t$ is the phase angle in delivery period *t*. (9) means the accumulated power from each generator should be bounded in each delivery period. (10) is the ramping constraint of the accumulated power from each generator for each delivery period, and (11) is the unit capacity constraint.

Because the line thermal limit is the soft constraint with risk, we use the quantile $q_{\alpha,lt}$ to quantify the potential loss for line *l* in period *t*. So the risk constraint in (2) is specified as (12) and (13):

$$q_{\alpha,lt}(f_{lt}-f_{l\max})\le Risk_{lt}: \ \tau_{tl}^{q,\max} \qquad \forall t,\forall l \quad (12)$$

$$q_{\alpha,lt}(f_{l\min}-f_{lt})\le Risk_{lt}: \quad \tau_{tl}^{q,\min} \qquad \forall t,\forall l \quad (13)$$

where $Risk_{lt}$ is the risk bound for line *l* in period *t*. $\tau_{lt}^{q,\max}$ and $\tau_{lt}^{q,\min}$ are dual variables. The state variable is the power flow $f_{lt}$. Constants are the lower and upper bounds of the line thermal limits $f_{l\min}$ and $f_{l\max}$ of line *l*. Thus, the full model of the IMRLD using the quantile as the risk metric is encapsulated by (7)-(13).

### *E. IMRLD model with the superquantile constraint*

If we use the superquantile instead of the quantile as the risk metric, the risk constraint in (2) is transformed to (14)-(16), rather than (12)-(13). In (14), the potential loss $L_{lt}$ in period *t* on line *l* is defined as a penalty when the power flow violates the thermal limit, shown as (14):

$$L_{lt}=\lambda_{lt}[f_{lt}-f_{l\max}]^{+}+\mu_{lt}[f_{l\min}-f_{lt}]^{+} \quad \forall t, \ \forall l \quad (14)$$

where $[\cdot]^{+}=\max(\cdot,0)$. $\lambda_{lt}$ and $\mu_{lt}$ are penalty prices when the power flow violates the thermal limit of line *l* in period *t*. The corresponding superquantile of the loss function $L_{lt}$ is given in (15):

$$\bar{q}_{\alpha lt}(L_{lt})=\frac{1}{1-\alpha}\int_{L_l\ge q_\alpha}L_{lt}\,p(\mathbf{w}_t)d\mathbf{w}_t, \ \forall l,\forall t \quad (15)$$

and the risk constraint is:

$$\bar{q}_{\alpha lt}(L_{lt})\le Risk_{lt}, \qquad \forall t,\forall l \quad (16)$$

Finally, the full model of the IMRLD using the superquantile as the risk metric is composed of (7)-(11) and (14)-(16).

Therefore, we see some features which make the IMRLD different from previous works. It is a multi-stage multi-period operational problem considering operational constraints and alternative risk metrics, so it can be used in the realistic power industry directly, compared with the BRLD and the related works [3], [12-15], [17], [18]. It also preserves the good features of the BRLD, so it achieves the global optimal decision like the BRLD.

## III. The Convexity of the IMRLD and the Model Solution

In this section, we first demonstrate the convexity of the IMRLD with the quantile and the superquantile risk metrics, so a local optimal solution would be global optimal. Then we prove a theorem mathematically to transform the IMRLD with the superquantile risk metric into a piece-wise linear programming problem. After solving these two technical challenges, the IMRLD can be finally computed by existing solvers like GUROBI.

### *A. The convexity of the IMRLD*

First of all, it should be noted that the BRLD in [3] is convex. We call the BRLD plus the hard constraints P1, and the BRLD plus the hard and soft constraints P2. According to the model formulation, the IMRLD is P2 in essence. For P1, one remark can be drawn, and is proved in Appendix A.

*Remark 1*: *P1 is a convex optimization problem.*

P2 is equal to P1 plus the soft constraints. For the quantile constraint, it can be reformed into a linear inequality if the prediction error of wind power is Gaussian distributed, and the convexity of the feasible region is thereby maintained according to the proof of *Remark 1*. The assumption of a Gaussian distribution for the prediction error of wind power is tenable as a result of the central limit theorem [31], and it has been widely used in the steady state operational problems [3].

For the superquantile constraint, it will not change the convexity of the feasible region because it is a coherent and convex risk metric. In addition, the superquantile constraint is always convex regardless of distributions, if the loss function is convex [36]. Therefore, P2, namely the IMRLD, is a convex optimization problem.

In this sense, the above models are both convex optimization problems, so a local optimal solution would global optimal.

### *B. Algorithm for solving the IMRLD problem*

For the model with the quantile constraint, we use (5) and the generator shifting matrix **A** to rewrite the risk constraint (12) and (13) to (17) and (18):

$$p(\mathbf{A}(\sum_{s=1}^{S}\mathbf{p}_{st}+\mathbf{w}_t+\mathbf{r}_{\mathrm{l}t}-\mathbf{d}_t-\mathbf{r}_{\mathrm{w}t})>\mathbf{f}_{\max})\le 1-\boldsymbol{\alpha}_t \quad \forall t \quad (17)$$

This article has been accepted for publication in a future issue of this journal, but has not been fully edited. Content may change prior to final publication. Citation information: DOI 10.1109/TII.2017.2651146, IEEE Transactions on Industrial Informatics



$$p(\mathbf{f}_{\min} - \mathbf{A}(\sum_{s=1}^{S}\mathbf{p}_{st} + \mathbf{w}_t + \mathbf{r}_{lt} - \mathbf{d}_t - \mathbf{r}_{wt}) > 0) \le 1-\boldsymbol{\alpha}_t \quad \forall t \quad (18)$$

These probability constraints are rewritten as the linear constraints using the thresholds $\boldsymbol{\varphi}_t^{\max}$ and $\boldsymbol{\varphi}_t^{\min}$ [37], based on the aforementioned assumptions.

$$\mathbf{A}(\sum_{s=1}^{S}\mathbf{p}_{st} + \mathbf{r}_{lt} - \mathbf{d}_t - \mathbf{r}_{wt}) \le \mathbf{f}_{\max} - \boldsymbol{\varphi}_t^{\max} : \ \boldsymbol{\tau}_t^{q,\max} \quad \forall t \quad (19)$$

$$\mathbf{A}(\sum_{s=1}^{S}\mathbf{p}_{st} + \mathbf{r}_{lt} - \mathbf{d}_t - \mathbf{r}_{wt}) \ge \mathbf{f}_{\min} - \boldsymbol{\varphi}_t^{\min} : \ \boldsymbol{\tau}_t^{q,\min} \quad \forall t \quad (20)$$

where $\boldsymbol{\tau}_t^{q,\max}$ and $\boldsymbol{\tau}_t^{q,\min}$ are the dual variables.

Moreover, the system power balance constraint is shown in (21):

$$\mathbf{1}^{\mathrm{T}}(\sum_{s=1}^{S}\mathbf{p}_{st} + \mathbf{w}_t + \mathbf{r}_{lt} - \mathbf{d}_t - \mathbf{r}_{wt}) = 0 \ : \ u_t \quad \forall t \quad (21)$$

where $u_t$ is the dual variable.

Therefore, the final IMRLD model with the quantile constraint includes (7), (9)-(11), and (19)-(21).

For the IMRLD with the superquantile constraint, it is challenging to solve it by existing solvers. Thus, we propose *Theorem 1* to reformulate the original problem into a piece-wise linear optimization problem.

*Theorem 1: The following two optimization problems generate the same efficient frontier:*

$$\begin{array}{ll} \text{(a)} \min\limits_{x} \ f(x,y) & \text{(b)} \min\limits_{x,\beta_i} \ f(x,y) \\ s.t \ \ \bar{q}_{\alpha i}[g_i(x,y)] \le Q_i, \forall i & s.t \ \ F_i[g_i(x,y),\beta_i] \le C_i, \forall i \end{array} \quad (22)$$

*where i is the index of constraints, $Q_i$ and $C_i$ are parameters, x is a deterministic variable, y is a random variable, and p(y) is the probability density function(PDF) of y. $\beta_i$ is an ancillary variable. $F(\cdot)$ is an ancillary function defined as:*

$$F(g(x,y),\beta) = \beta + \frac{1}{1-\alpha}\int [g(x,y)-\beta]^+ p(y)dy \quad (23)$$

The proof of *Theorem* 1 is provided in Appendix B.

Thus, we define the ancillary function for our specific problem as:

$$\begin{aligned} &F_{lt}(\mathbf{p}_{st},\mathbf{r}_{lt},\mathbf{w}_t,\mathbf{r}_{wt},\beta_{lt}) = \beta_{lt} + \\ &\frac{1}{(1-\alpha_{lt})}\int [\lambda_{lt}[\mathbf{a}_l(\sum_{s=1}^{S}\mathbf{p}_{st} + \mathbf{w}_t + \mathbf{r}_{lt} - \mathbf{d}_t - \mathbf{r}_{wt}) - \mathbf{f}_{\max}]^+ + \\ &\mu_{lt}[\mathbf{f}_{\min} - \mathbf{a}_l(\sum_{s=1}^{S}\mathbf{p}_{st} + \mathbf{w}_t + \mathbf{r}_{lt} - \mathbf{d}_t - \mathbf{r}_{wt})]^+ - \beta_{lt}]^+ \ p(\mathbf{w}_t)d\mathbf{w}_t \end{aligned} \quad (24)$$

where $\mathbf{a}_l$ is the $l^{\text{th}}$ row of the generator shifting matrix **A.** The vector $\mathbf{f}_{\max}$ and $\mathbf{f}_{\min}$ are the bounds of the thermal limits. According to *Theorem 1*, the optimization problem (7)-(11), and (14)-(16) is equivalent to (7), (9)-(11), (21) and (25) where:

$$F_{lt}(\mathbf{p}_{st},\mathbf{r}_{lt},\mathbf{w}_t,\mathbf{r}_{wt},\beta_{lt}) \le Risk_{lt}, \quad \forall t, \forall l \quad (25)$$

Furthermore, if we use discrete samples to represent the random variable $\mathbf{w}_t$, (25) can be discretized to (26) for any type of distribution [36]:

$$\begin{aligned} &\beta_{lt} + \sum_{k=1}^{K}\frac{1}{k(1-\alpha)} \times [\lambda_{lt}[\mathbf{a}_l(\sum_{s=1}^{S}\mathbf{p}_{st} + \mathbf{w}_{tk} + \mathbf{r}_{lt} - \mathbf{d}_t - \mathbf{r}_{wtk}) \\ &-\mathbf{f}_{\max}]^+ + \mu_{lt}[\mathbf{f}_{\min} - \mathbf{a}_l(\sum_{s=1}^{S}\mathbf{p}_{st} + \mathbf{w}_{tk} + \mathbf{r}_{lt} - \mathbf{d}_t - \mathbf{r}_{wtk})]^+ \\ &-\beta_{lt}]^+ \le Risk_{lt} \ : \ \tau_{lt}^{sq} \qquad \forall t, \forall l \end{aligned} \quad (26)$$

where $k$ is the index of the samples, and $\tau_{lt}^{sq}$ is the dual variable.

Therefore, the objective of the final IMRLD with superquantile constraint is to minimize (7), subject to (9)-(11), (21) and (26). It is a piece-wise linear optimization, which can be efficiently computed by existing solvers.

## IV. Locational Marginal Price Analysis

In order to analyze the IMRLD model, the LMP is derived in this section to reveal the relation between the marginal operational cost and the uncertainty from renewables injections. In addition, the LMP analysis also contributes to the detection of transmission congestions in a network.

In our formulation, we cannot obtain the LMP by checking the dual variables directly, because the nodal power balance equation is not explicit. In this regard, the LMP is derived by perturbing the load in the Lagrangian function of the IMRLD. The Lagrangian functions of the IMRLD with the quantile and the superquantile constraints are denoted as $l_1$ and $l_2$ respectively. A perturbation $\xi_{nt}$ on load at bus $n$ in period $t$ is used, in order to derive an analytical form of the LMP.

### A. LMP of the IMRLD with the quantile constraint

For node $n$ in delivery period $t$, the LMP is derived in (27):

$$LMP_{nt} = \frac{\partial l_1}{\partial \xi_{nt}} = u_t - \sum_{l=1}^{L}\tau_{tl}^{q,\max}a_{ln} + \sum_{l=1}^{L}\tau_{tl}^{q,\min}a_{ln} \quad (27)$$

where $a_{ln}$ is the entry of matrix **A**, $L$ is the number of lines, $u_t$, $\tau_{lt}^{q,\max}$ and $\tau_{lt}^{q,\min}$ are the dual variables of constraint (21), (12) and (13).

The first component in (27) is interpreted as the marginal operational cost of the reference bus, not depending on transmission lines. The second and the third components stand for the marginal cost of congestion. The impact of the operational risk can be treated as an expansion of the transmission capacity determined by the thresholds $\boldsymbol{\varphi}_t^{\max}$ and $\boldsymbol{\varphi}_t^{\min}$. In this sense, the congestion cost of the expanded transmission line is equal to the merchandizing surplus. In addition, if $\xi_{nt}$ is interpreted as wind perturbation, the LMP is the price of wind power at bus $n$ in period $t$. It should be mentioned that the uncertainty is implicitly included in the Lagrangian multipliers $u_t$, $\tau_{lt}^{q,\max}$ and $\tau_{lt}^{q,\min}$.

### B. LMP of the IMRLD with the superquantile constraint

For node $n$ in delivery period $t$, the LMP is derived in (28):

$$LMP_{nt} = \frac{\partial l_2}{\partial \xi_{nt}} = u_t + \sum_{l=1}^{L}\frac{\tau_{lt}^{sq}}{1-\alpha_{lt}}\frac{\partial \int_{L_{lt}\ge q_\alpha} L_{lt}\,p(\mathbf{w}_t)d\mathbf{w}_t}{\partial \xi_{nt}} \quad (28)$$

where $\tau_{lt}^{sq}$ is the dual variable of (26).

Akin to (27), the first component reflects the marginal cost of the reference bus, while the second component stands for the congestion price relative to the reference bus. Moreover, if the wind power output follows a joint Gaussian distribution, the LMP can be further simplified as:

$$LMP_{nt} = u_t + \sum_{l=1}^{L}\frac{\tau_{lt}^{sq}[\mathrm{I}_1(\mu_{lt}a_{ln}) - \mathrm{I}_2(\lambda_{lt}a_{ln})]}{(1-\alpha_{lt})}P(w \ge W) \quad (29)$$

In (29), $P$ denotes a joint probability, $w$ is an ancillary random variable, and $W$ is a threshold derived in Appendix C.

This article has been accepted for publication in a future issue of this journal, but has not been fully edited. Content may change prior to final publication. Citation information: DOI 10.1109/TII.2017.2651146, IEEE Transactions on Industrial Informatics



Indicator functions $I_1$ and $I_2$ equal to $\mu_{lt}a_{ln}$ and $\lambda_{lt}a_{ln}$ when the values of the second and the third line in (26) are not zero respectively. (Otherwise, $I_1$ and $I_2$ are zero)

If we can find a threshold like the case in the quantile model, the effect of the operational risk on the transmission capacity can also be deemed as an expansion of transmission lines. However, for the superquantile case, it is difficult to calculate such a threshold, so we need the reformulation and *Theorem* 1 to solve the model. In addition, the LMP is explicitly related to the joint probability distribution, so it is possible to analyze the effect of wind forecast error on the LMP directly.

## V. Case Study

In this section, two case studies are conducted for the IMRLD. The first case is based on a modified IEEE 6-bus system, and the second case is based on a realistic wind power system from Gansu province of China. The models for these cases are coded in CVX 2.1 in MATLAB 2013 and solved by GUROBI 6.0. All experiments are conducted on a PC Dell OPTIPLEX 9010 with Intel Dual Core i5 at 3.30, 3.30 GHz and 128 GB RAM in a 64-bit Windows 7 operating system.

### A. A modified IEEE standard system

The first case is based on a modified IEEE 6-bus system with 3 dispatch stages (S1, S2 and S3) and 3 delivery periods (T1, T2 and T3). All system data can be found in [33]. In this case, the prediction data of the wind are generated by Monte Carlo simulation based on the joint Gaussian distribution with 1000 samples. Mean values of the two wind plants are given in Table I. ($x$/$y$) in Table I represents the mean values of the wind power at bus 2 and bus 3 respectively. The covariance matrix represents the prediction error. Table II gives the covariance matrix in high prediction error (HPE), medium prediction error (MPE) and low prediction error (LPE) for this case.

TABLE I
Mean Values of the Wind Power at Bus 2 and Bus 3

| W2/W3 (MW) | T1 | T2 | T3 |
|---|---|---|---|
| S1 | 10/9.4 | 15.3/11.2 | 25.3/20.3 |
| S2 | 10/7.7 | 14.4/11.1 | 20.9/19.9 |
| S3 | 10/5.8 | 15/8.8 | 23.3/15.3 |

TABLE II
Covariance Matrix in HPE, MPE and LPE

| | HPE | MPE | LPE |
|---|---|---|---|
| S1 | [10,6;6,10] | [5,2;2,5] | [2,1;1,2] |
| S2 | [6,3;3,2] | [2,1;1,2] | [1, 0.5; 0.5, 1] |
| S3 | [0,0;0,0] | [0,0;0,0] | [0,0;0,0] |

There are three objectives in this case. The first objective illustrates how the IMRLD generates the scheduling plan of each unit at each dispatch stage for each delivery period. Based on the scheduling plan, the second objective compares the operational costs among the traditional deterministic operation (TD), the three-stage stochastic programming (SP) and the IMRLD. The last objective analyzes the IMRLD model to find the relation between the operational cost, the system flexibility, the prediction error and the wind penetration level.

*Objective A1*: assume the prediction error is LPE. Based on the data in Table I and Table II, the scheduling plans of each unit at each dispatch stage for each delivery period of the quantile and the superquantile models are computed by (7)-(11), (14)-(16), and (7), (9)-(11), (21), (26) respectively. The output of unit 3 is always zero because of its high operational cost. The outputs of unit 1 and 2 are shown in Table III, and (*N*/*M*) in Table III are the outputs computed by the quantile and the superquantile model respectively.

TABLE III
Operational Schedules of Unit 1 and Unit 2

| Quantile/Superquantile | | S1 | S2 | S3 |
|---|---|---|---|---|
| Unit1 (MW) | T1 | 98.3/98.5 | 0/0 | 0/0 |
| | T2 | 108.7/110.4 | 0/0 | 0/0 |
| | T3 | 117.2/120.9 | 0/0 | 0/0 |
| Unit2 (MW) | T1 | 94.4/97.4 | 1.1/1.9 | 0.4/0.6 |
| | T2 | 76.9/80.3 | 0.4/0.5 | 0.2/0.3 |
| | T3 | 49.3/51.8 | 4.2/4.3 | 0.7/1.1 |

In Table III, operators purchase power at dispatch stage 1, and purchase recourse power at dispatch stage 2 because the change of prediction is known, given in Table I and II. Similarly, additional power will be purchased at the last stage.

*Objective A2*: the wind data is represented by the mean values in Table I without prediction errors in the TD. In the SP and the IMRLD, the wind data are given in Table I and II. Table IV shows the operational costs of the TD, SP and IMRLD. (*N*/*M*) in Table IV are the operational costs computed by the quantile and the superquantile model respectively.

TABLE IV
Operational Costs of the TD, SP and IMRLD

| | S1 | S2 | S3 | Total |
|---|---|---|---|---|
| TD($/hr) | 6,472.8 | 0 | 465.5 | 6,938.3 |
| SP($/hr) | 6,618.1 | 179.7 | 69.2 | 6,867.0 |
| IMRLD($/hr) | 6,495.7 /6,551 | 80.3 /142.5 | 24.4 /45.5 | 6,600.4 /6,739 |

Table IV shows the operational costs of the TD, SP and IMRLD at each dispatch stage. Compared with the TD, the IMRLD takes advantage of the available prediction information of the wind power decreasing so it avoids buying much power at the last stage with a very high price. Moreover, operators can correct the operational decision in the recourse stage with a lower price. Compared with the 3-stage SP, the permission of the operational risk at stage 1 and 2 within a given risk level leads to the lower operational cost in the IMRLD. In addition, more power would be purchased in the superquantile model and the operational cost is thereby higher because the severity and probability of losses are both integrated in the superquantile model, whereas the quantile model just considers the probability of losses.

Table V compares the performance of each model. It is found that there are more variables and constraints in the superquantile model, which is more computationally expensive.

TABLE V
Performance Comparison of the Modified 6-bus System

| | Quantile model | Superquantile model |
|---|---|---|
| Number of variables | 102,204 | 188,206 |
| Number of constraints | 87,132 | 106,133 |
| CPU time | 20.83s | 186.67s |

In sum, we draw one note from the above observations:

This article has been accepted for publication in a future issue of this journal, but has not been fully edited. Content may change prior to final publication. Citation information: DOI 10.1109/TII.2017.2651146, IEEE Transactions on Industrial Informatics



*Note A1: the IMRLD has a lower operational cost compared with the TD and SP, because it preserves the good features of the BRLD.*

*Objective A3*: there are three scenarios. The base case for all scenarios is the system without any wind power injection, denoted by the blue line in the figures. The overall system flexibility is defined as the system upward/downward ramping capability in 10 minutes. For example, system flexibility equals to 10%/10mins means units can ramp upward/downward 10% of their total capacity in 10 minutes. The penetration level is the wind power capacity over the total installed capacity.

Scenario 1: set the system flexibility level to 20%/10mins. This scenario finds the relation between the wind penetration level, the wind prediction error, and the operational cost. There are three subcases in this scenario for the quantile and the superquantile models: HPE, MPE and LPE, shown in Fig. 3(a).

Scenario 2: set the prediction error to MPE. This scenario finds the relation between the wind penetration level, the system flexibility, and the operational cost. There are 3 subcases in this scenario for both the quantile and superquantile models: high system flexibility (HSF), medium system flexibility (MSF) and low system flexibility (LSF), shown in Fig. 4(a). Based on the definition of the system flexibility, HSF, MSF and LSF are chosen as 40%/10mins, 20%/10mins and 10%/10mins.

Scenario 3: set the penetration level to 20%. This scenario finds the relation between the system flexibility, the wind prediction error, and the operational cost. Again, there are 3 subcases in this scenario for both the quantile and superquantile models: HPE, MPE and LPE, shown in Fig. 4(b).

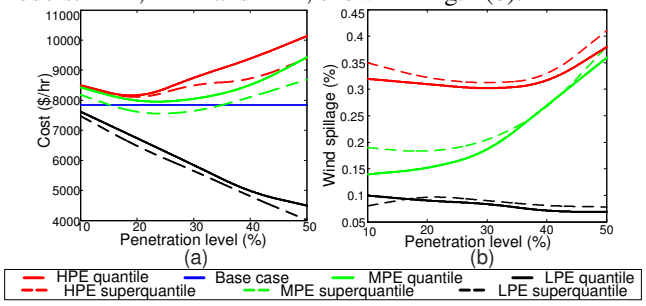


Fig. 3. (a) Given the flexibility level, the relationship between the wind penetration and the prediction accuracy. (b) The wind spillage in scenario 1.

For both scenario 1 and scenario 2 shown in Fig. 3(a) and Fig. 4(a), the characteristics of the curves are similar: (a) In the HPE and MPE subcases, or the HSF and MSF subcases, it is not surprising that the costs first drop down with the increased penetration level. When the penetration levels reach about 20% in scenario 1 and 25% in scenario 2, the curves start to rise. Because the deviation of the prediction leads to a much more severe shortage of the reserve at the real time when the penetration level is high, more power must be purchased at the last stage with a high price. However, in the LPE and LSF subcase, the costs decrease monotonously with the penetration levels. (b) For each curve, the part beyond the base case means the operational cost of a wind power system is higher than the cost of a system without wind. The inaccurate forecast results in insufficient power purchasing at the stage with a low price, so it leads to the excessive purchase at the real time. (c) The cost of the superquantile model is higher than the quantile model, given the same confidential levels and risk parameters. In addition, Fig. 3(b) provides the wind spillage in each subcase. The high wind spillage percentages in the HPE and MPE reveal that the high penetration level does not necessarily provide economic profits without matched forecast technology and system flexibility.

Nevertheless, for the scenario 3 shown in Fig. 4(b), shapes of the curves are different: (a) For the HPE and MPE, the costs slope down when the flexibility improves. The suitable flexibility is about 25%/10mins and 43.5%/10mins respectively to hold the wind power. (b) In the LPE subcase, the costs barely decline, because the prediction is precise enough so that the uncertainty of the wind can be handled by a comparatively low flexibility level.

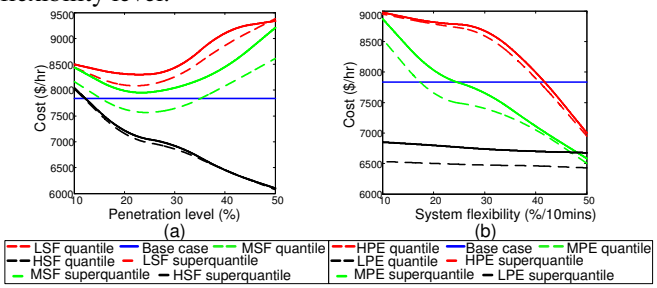


Fig. 4. (a) Given the prediction accuracy, the relationship between the wind penetration and the flexibility. (b) Given the penetration level, the relationship between the flexibility and the prediction accuracy.

In sum, the above observations and analysis give rise to one note:

*Note A2: impact factors in the IMRLD are coupling. Analysis of the IMRLD shows the wind power integration will probably bring no economic benefits without matched prediction accuracy and system flexibility.*

### *B. The realistic system in Gansu, China*

In the second case, the simulation is built on a realistic system, the Gansu power grid in China, which has a large-scale wind power integration. There are 132 buses and 244 transmission lines in the system. The wind power injects at bus 14, 38, 51, 63, 54 and 58, and 1000 samples of wind power are generated and reduced to 10 samples with sophisticated scenario reduction tool [39]. Details of this system can be found in [33].

The objectives of this case are twofold: (1) Compare the operational costs between the TD, SP and IMRLD for the Gansu realistic system. (2) Illustrate the LMP calculation of all 750kV buses and find the reason for the variation in the LMPs over the total 12 delivery periods.

*Objective B1*: the comparison between the TD, SP and IMRLD for the Gansu realistic system is shown in Table VI.

TABLE VI
COMPARISON OF THE OPERATION COSTS FOR THE REALISTIC SYSTEM

| | S1 | S2 | S3 | Total |
|---|---|---|---|---|
| TD($/hr) | 22,319.7 | 0 | 10,513.9 | 32,834.6 |
| SP($/hr) | 22,819.7 | 7,332.4 | 205.1 | 30,357.2 |
| IMRLD($/hr) | 22,684.0 /22,736.6 | 6,718.3 /7,053.7 | 55.9 /106 | 29,458.2 /29,896.3 |

Table VI shows the similar result with Table V on the 6-bus

This article has been accepted for publication in a future issue of this journal, but has not been fully edited. Content may change prior to final publication. Citation information: DOI 10.1109/TII.2017.2651146, IEEE Transactions on Industrial Informatics



system. The IMRLD has the lowest operational cost. Compared with the TD, the economic benefits of the IMRLD come from the utilization of recourse stage to correct the operational decision. Compared with the SP, some extreme scenarios are not considered because of the acceptable operational risk level, so the operational cost of the IMRLD is lower. Table VI can be concluded to one note:

*Note B1: the IMRLD has a lower operational cost than the TD and SP for the realistic Gansu power system, because it preserves the good features of the BRLD.*

The performance of the IMRLD for the realistic system is provided in Table VII. There are more variables in the superquantile model, thus it needs more CPU time. In addition, provided more advanced solvers and computers, if any, the number of samples and the problem scale can be further enlarged to render a better operational plan, and the computational time can be further reduced.

TABLE VII
PERFORMANCE COMPARISON OF THE REALISTIC SYSTEM

| | Quantile model | Superquantile model |
|---|---|---|
| Number of variables | 108,864 | 167,566 |
| Number of constraints | 22,176 | 86,939 |
| CPU time | 40.83s | 266.32s |

For the LMP analysis, the mean values of wind power predicted at the first stage are shown in Fig. 5. At time $t$=5, $t$=8 and $t$=10, the wind power ramps up while sinks down at $t$=6, $t$=9 and $t$=11.

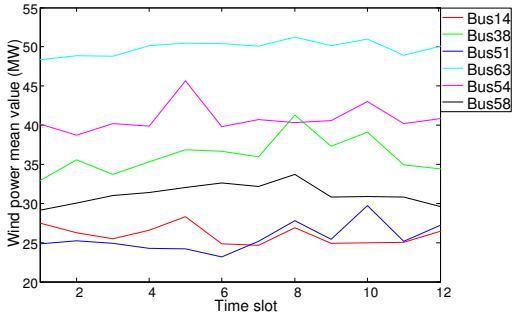


Fig. 5. The predicted mean values of the wind power at the first stage.

The LMPs of the quantile model and the superquantile model are shown in Fig. 6.

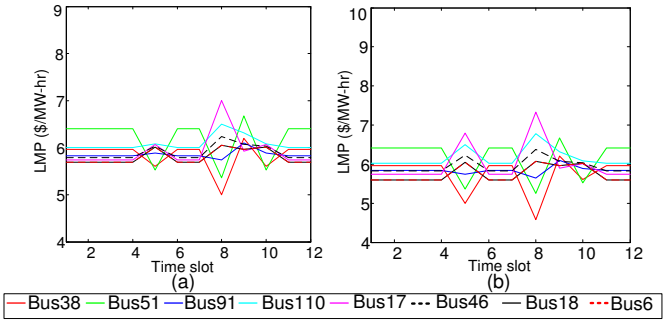


Fig. 6. (a) The LMPs in the quantile model. (b) The LMPs in the superquantile model.

Some heuristic and impressive features can be found in Fig. 6. At the first glance, there are 3 peaks of the LMPs at $t$=5, $t$=8 and $t$=10, coincident with the wind power peaks. The largest LMP fluctuations are at bus 17, 38 and 51. Intuitively, the raise of wind power will result in cost-saving, just like the fact at bus 38 and 51 where the LMPs tumble down. However, the LMP of bus 17 paradoxically increases with the wind power. This abnormal phenomenon results from the different location of the buses and line congestions. Because bus 38 and 51 are wind injection point, the LMPs decline. But the congested lines in the system are increased due to the increment of the wind power injection at $t$=5, $t$=8 and $t$=10, thus the LMPs of some buses rise up with nuanced degrees. For bus 17, the sharp ascent of the LMP is due to the neighboring congested lines. However for the other buses, the LMPs slightly grow because they are far from the congested area.

In normal condition, the free price of the wind power will reduce the LMP intuitively. However, this is not the case for some buses in the realistic Gansu power system. This abnormal situation is concluded by the following note:

*Note B2: line congestions in the Gansu power system lead to the rise of the LMPs in some buses even when the wind power increases.*

## VI. CONCLUSION

In conclusion, the paper proposes the IMRLD as a power system operational method for the renewables integration, because it preserves the advantages of the BRLD, and it satisfies the three realistic industrial requirements simultaneously. The convexity is verified and a theorem is proved to make the IMRLD solvable. The LMP is then derived to analyze the relation between the system marginal operational cost and the uncertainty from the renewables injection.

The case studies on a modified IEEE 6-bus system and a realistic provincial system in China demonstrate the economic benefits of the IMRLD. In addition, the simulation result of the IMRLD shows that the impact factors of the operational cost, which are the system flexibility, the wind penetration level, and the prediction accuracy, are coupling. The operational cost of a system with wind power integration may be higher than the system without wind, if the prediction accuracy and the system flexibility are not matched. Lastly, the LMP analysis shows that the limited transmission capacity is another factor that prevents the economic benefits of wind power integration.

## APPENDIX

### A. *Proof of Remark 1*

The hard constraints are a set of linear inequalities and equalities, denoted in (30):

$$\begin{aligned} a_i^T x \le b_i, \quad & i \in \mathrm{A}_1 \\ c_j^T x = d_j, \quad & j \in \mathrm{A}_2 \end{aligned} \tag{30}$$

where $a$, $b$, $c$ and $d$ are parameters, $i$ and $j$ are the index of the inequalities and equalities, and A1, A2 are the sets of inequalities and equalities.

For the linear equalities, they are rewritten into a set of inequalities shown as:

$$c_j^T x \le d_j, c_j^T x \ge d_j, \ j \in \mathrm{A}_2 \tag{31}$$

Therefore, the hard constraints can be reformed into a set of linear inequalities:

This article has been accepted for publication in a future issue of this journal, but has not been fully edited. Content may change prior to final publication. Citation information: DOI 10.1109/TII.2017.2651146, IEEE Transactions on Industrial Informatics



$$e_k^T x \le f_k, \quad k \in \mathrm{A}_3 \tag{32}$$

where $e$ and $f$ are parameters, $k$ is the index of the inequalities, and $\mathrm{A}_3$ is the set of inequalities.

Assume $x$, $y$ be two solutions of (32), we have

$$\begin{aligned} e_k^T x \le f_k, \quad k \in \mathrm{A}_3 \\ e_k^T y \le f_k, \quad k \in \mathrm{A}_3 \end{aligned} \tag{33}$$

If the inequalities are multiplied by nonnegative values $q$ and 1-$q$, we have:

$$qe_k^T x + (1-q)e_k^T y \le qf_k + (1-q)f_k = f_k, \quad k \in \mathrm{A}_3 \tag{34}$$

(34) means any point $z=qx+(1-q)y$ is a solution to (32), provided $q \in [0,1]$. Therefore, the feasible region composed of the hard constraints is a convex set.

### B. Proof of Theorem 1

*Prerequisite 1: The following optimization problems are equivalent, if $f(x,y)$ and $g(x,y)$ are convex* [36].

$$\begin{aligned} &\text{(a)} \min_{x \in \Psi} \ f(x,y) + a\bar{q}_\alpha[g(x,y)] \\ &\text{(b)} \min_{x \in \Psi, \beta} \ f(x,y) + aF[g(x,y),\beta] \end{aligned} \tag{35}$$

*where $\Psi$ is a feasible region of the deterministic variable x. y is a random variable. a is a parameter, $F(\cdot)$ is the ancillary function defined in* [36]*, and $\beta$ is the ancillary variable.*

*Prerequisite 2: The following optimization problems generate the same efficient frontier, when $f(x)$ is convex and $g(x)$ is concave* [38].

$$\begin{aligned} &\text{(a)} \min \ f(x) && \text{(b)} \min f(x) + ag(x) \\ &s.t. \ \ g(x) \le G, \ x \in \Psi && s.t. \ \ x \in \Psi \end{aligned} \tag{36}$$

*where a and G are parameters.*

By *Prerequisite 2*, the two problems below generate the same efficient frontier:

$$\begin{aligned} &\text{(a)} \min_x \ f(x,y) && \text{(b)} \min_x f(x,y) + a_1\bar{q}_{\alpha 1}[g_1(x,y)] \\ &s.t \ \ \bar{q}_{\alpha i}[g_i(x,y)] \le Q_i, \forall i && s.t \ \ \bar{q}_{\alpha i}[g_i(x,y)] \le Q_i, \forall i \ne 1 \end{aligned} \tag{37}$$

where $Q_i$ and $a_1$ are parameters. By *Prerequisite 1*, the two problems below are equivalent:

$$\begin{aligned} &\text{(a)} \min_x \ f(x,y) && \text{(b)} \min_x f(x,y) + a_1\bar{q}_{\alpha 1}[g_1(x,y)] \\ &s.t \ \ \bar{q}_{\alpha i}[g_i(x,y)] \le Q_i, \forall i && s.t \ \ \bar{q}_{\alpha i}[g_i(x,y)] \le Q_i, \forall i \ne 1 \end{aligned} \tag{38}$$

By *Prerequisite 2*, the two problems below generate the same efficient frontier, where $C_1$ is a parameter:

$$\begin{aligned} &\text{(a)} \min_{x,\beta_1} f(x,y) + a_1 F_1[g_1(x,y),\beta_1] && \text{(b)} \min_{x,\beta_1} f(x,y) \\ &s.t \ \ \bar{q}_{\alpha i}[g_i(x,y)] \le Q_i, \forall i \ne 1 && s.t \ \ \bar{q}_{\alpha i}[g_i(x,y)] \le Q_i, \forall i \ne 1 \\ & && F_1[g_1(x,y),\beta_1] \le C_1 \end{aligned} \tag{39}$$

With (37)-(39), all the superquantile constraints can be transformed to the ancillary functions, thus *Theorem 1* can be proved.

### C. Derivation of the LMP for the superquantile model

When the optimization problem of the superquantile model is solved, the loss function and the ancillary function degenerate into an affine function. Assume the wind power is subject to a joint Gaussian probability, the lower limit of the integral in (28) can be analytically expressed as:

$$\mathbf{a}_l \mathbf{w}_t \ge \mu_w + \varphi_\alpha \sigma_w \tag{40}$$

where $\mu_w$ and $\sigma_w$ are the mean and the variance of the PDF of $\mathbf{a}_l\mathbf{w}_t$, and $\varphi_\alpha$ is the $\alpha$-quantile of the normal distribution. Thus,

$$\begin{aligned} &\frac{\partial \int_{L_{lt} \ge q_\alpha} L_{lt} p(\mathbf{w}_t) d\mathbf{w}_t}{\partial \xi_{nt}} = [\mathrm{I}_1(\mu_{lt} a_{ln}) - \mathrm{I}_2(\lambda_{lt} a_{ln})] \\ &\times \int_{\mathbf{a}_l \mathbf{w}_t \ge \mu_w + \varphi_\alpha \sigma_w} p(\mathbf{w}_t) d\mathbf{w}_t \end{aligned} \tag{41}$$

The integral is actually a probability, which can be calculated and denoted by $P(w \ge W)$.

Finally, substituting (41) into (28), the LMP of the IMRLD with the superquantile risk metric becomes:

$$LMP_{nt} = u_t + \sum\nolimits_{l=1}^{L} \frac{\tau_{lt}^{sq}[\mathrm{I}_1(\mu_{lt} a_{ln}) - \mathrm{I}_2(\lambda_{lt} a_{ln})]}{(1-\alpha_{lt})} P(w \ge W) \tag{42}$$

## ACKNOWLEDGMENT

The authors would like to thank Professor Felix F. Wu with the University of California, Berkeley for the valuable discussion. The authors would like to thank Professor Ningbo Wang with Gansu power grid for data support. The authors would also like to thank editor and reviewers for their valuable suggestions for improving the quality of this paper.

## REFERENCES

[1] A. Papavasiliou, S. S. Oren, and R. P. O'Neill, "Reserve requirements for wind power integration: A scenario-based stochastic programming framework," *IEEE Trans. Power Syst.,* vol. 26, no. 4, pp. 2197-2206, Nov. 2011

[2] L. Xie, P. M. S. Carvalho, L. A. F. M. Ferreira, J. Liu, B. H. Krogh, N. Popli*, et al.*, "Wind integration in power systems: Operational challenges and possible solutions," *Proc. IEEE,* vol. 99, no. 1, pp. 214-232, Jan. 2011

[3] P. P. Varaiya, F. F. Wu, and J. W. Bialek, "Smart operation of smart grid: Risk-limiting dispatch," *Proc. IEEE,* vol. 99, no. 1, pp. 40-57, Jan. 2011

[4] C. Peng, S. Lei, Y. Hou and F. Wu, "Uncertainty management in power system operation," *CSEE J. Power and Energy Syst.,* vol. 1, no. 1, pp. 28-35, May 2015

[5] North American Electric Reliability Corporation, "Integrated Bulk Power System Risk Assessment Concepts," 2010

[6] PJM, "PJM eMKT User Guide," 2015

[7] S. C. Muller, U. Hager, C. Rehtanz, "A multiagent system for adaptive power flow control in electrical transmission systems," *IEEE Trans. Ind. Informat.,* vol. 10, no. 4, pp. 2290-2299, April 2014

[8] Y. Xu, W. Zhang, and W. Liu, "Distributed dynamic programming-based approach for economic dispatch in smart grids," *IEEE Trans. Ind. Informat.,* vol. 11, no .1, pp. 166-175, Jan. 2015

[9] M. Benidris and J. Mitra, "Reliability and sensitivity analysis of composite power systems under emission constraints," *IEEE Trans. Power Syst.,* vol. 29, no. 1, pp. 404-412, Jan. 2014

[10] N. Yu, A. Somani, and L. Tesfatsion, "Financial risk management in restructured wholesale power markets: Concepts and tools," in *Proc. 2010 IEEE Power & Energy Society General Meeting*, July 2010

[11] D. Nguyen and L. Le, "Risk-constrained profit maximization for microgrid aggregators with demand response," *IEEE Trans. Smart Grid,* vol. 6, no. 1, pp. 135-146, Jan. 2015

[12] R. Rajagopal, E. Bitar, P. Varaiya, and F. Wu, "Risk-limiting dispatch for integrating renewable power," *Int. J. Elec. Power,* vol. 44, no. 1, pp. 615-628, Jan. 2013

[13] J. Qin, B. Zhang, and R. Rajagopal, "Risk limiting dispatch with ramping constraints," in *Proc. 2013 IEEE International Conference Smart Grid Communications* (*SmartGridComm*), Oct. 2013

[14] J. Qin, I. S. Han, and R. Rajagopal, "Storage in risk limiting dispatch: control and approximation," in *Proc. 2013 American Control Conference* (*ACC*), Jun. 2013

[15] B. Zhang, R. Rajagopal, and D. Tse, "Network risk limiting dispatch: optimal control and price of uncertainty," *IEEE Trans. Autom. Control,* vol. 59, no .9, pp. 2442-2456, Sep. 2014

[16] R. Piwko, P. Meibom, H. Holttinen, B. Shi, N. Miller, Y. Chi, *et al.*, "Penetrating insights: lessons learned from large-scale wind power integration," *IEEE Power and Energy Mag.,* vol. 10, no. 2, pp. 44-52, Feb.2012
[17] G. Huang, Y. Wen, Y. Bao, C. Guo, S. Ma, and Q. He, "Comprehensive decoupled risk-limiting dispatch," in *Proc. 2015 IEEE Power & Energy Society General Meeting*, July 2015
[18] C. Wu, G. Hug, and S. Kar, "Risk-limiting economic dispatch for electricity markets with flexible ramping products," *IEEE Trans. Power Syst.,* vol. 31, no. 3, pp. 1990-2003, Aug. 2015
[19] J. M. Morales, A. J. Conejo, H. Madsen, P. Pinson and M. Zugno, *Integrating Renewables in Electricity Markets*, Springer, 2014
[20] D. S. Kirschen, G. Strbac, *Fundamentals of Power System Economics*, Wiley, 2004
[21] National Renewable Energy Laboratory, Argonne National Laboratory, "Evolution of Wholesale Electricity Market Design with Increasing Levels of Renewable Generation", 2014
[22] M. Rahimiyan, L. Baringo, "Strategic bidding for a virtual power plant in the day-ahead and real-time markets: a price-taker robust optimization approach", *IEEE Trans. Power Syst.*, vol. 31, no. 4, pp. 2676-2687, July 2016
[23] A. A. Sanchez de la Nieta, J. Contreras, J. I. Munoz, and M. O'Malley, "Modeling the impact of a wind power producer as a price-maker," *IEEE Trans. Power Syst.,* vol. 29, no. 6, pp. 2723-2732, Nov. 2014
[24] Midcontinent Independent System Operator, "Demand Curves for Transmission Constraints," 2013
[25] North American Electric Reliability Corporation, "Reliability Concepts V. 1.0.2," 2007.
[26] X. Li, X. Zhang, L. Wu, P. Lu and S. Zhang, "Transmission line overload risk assessment for power systems with wind and load-power generation correlation", *IEEE Trans. Smart Grid*, vol. 6, no. 3, pp. 1233-1242, May 2015
[27] M. Ni, J. D. McCally, V. Vittal and T. Tayyib, "Online risk-based security assessment", *IEEE Trans. Power Syst.*, vol. 18, no. 1, pp. 258-265, Feb. 2003
[28] B. Stott, J. Jardim and O. Alsac, "DC power flow revisited," *IEEE Trans. Power Syst.*, vol. 24, no. 3, pp. 1290-1300, May 2009
[29] Midcontinent Independent System Operator, "Financial Transmission Rights and Auction Revenue Rights," 2011.
[30] H. Gangammanavar, S. Sen and V. Zavala, "Stochastic optimization of sub-hourly economic dispatch with wind energy," *IEEE Trans. Power Syst.*, vol. 31, no. 2, pp. 949-959, Mar. 2016
[31] R. T. Rockafellar and J. O. Royset, "Risk measures in engineering design under uncertainty," in *Proc. 12th International Conference on Applications of Statistics and Probability in Civil Engineering*, 2015
[32] Northwest Power And Conservation Council, "Review of Supply Adequacy Criteria in the Northwest," 2011
[33] Wind Power Simulation Data. [Online] Available: http://www.eee.hku.hk/~yhhou/Wind%20Power%20Simulation%20Systems.pdf
[34] A. Bensoussan, P. R. Bertrand and A. Brouste, "Forecasting the energy produced by a windmillon a yearly basis," *Stoch. Env. Res. Risk A.*, vol. 26, pp. 1109-1122, Mar. 2012
[35] S. Ahmed and A. Shapiro, "Solving Chance-Constrained Stochastic Programs via Sampling and Integer Programming," 2008
[36] R. T. Rockafellar, S. Uryasev "Optimization of conditional value at-risk," *J. Risk,* vol. 2, pp. 21-41, 2000
[37] S. Boyd and L. Vandenberghe, *Convex Optimization*: New York: the United States of America by Cambridge University Press, 2004
[38] J. Palmquist, S. Uryasev and P. Krokhmal, "Portfolio optimization with conditional value at risk objective and constraints," *J. Risk,* Vol. 4, 2002, pp. 11-27
[39] GAMS/SCENRED Documentation, Nov. 2013

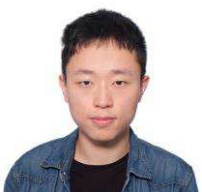

**Chaoyi Peng** (S'13) received the B.E. degree from Huazhong University of Science and Technology, Wuhan, China, in 2012. He is currently pursuing the Ph.D. degree in The University of Hong Kong, Hong Kong. His research interests include operation optimization, resilience, and renewables integration in power systems.

**Yunhe Hou** (M'08-SM'15) received the B.E. and Ph.D. degrees in electrical engineering from Huazhong University of Science and Technology, Wuhan, China, in 1999 and 2005, respectively.

He was a Post-Doctoral Research Fellow at Tsinghua University, Beijing, China, from 2005 to 2007, and a Post-Doctoral Researcher at Iowa State University, Ames, IA, USA, and the University College Dublin, Dublin, Ireland, from 2008 to 2009. He was also a Visiting Scientist at the Laboratory for Information and Decision Systems, Massachusetts Institute of Technology, Cambridge, MA, USA, in 2010. He joined the faculty of the University of Hong Kong, Hong Kong, in 2009, where he is currently an Assistant Professor with the Department of Electrical and Electronic Engineering.

Dr. Hou is an Editor of the IEEE Transactions on Smart Grid and an Associate Editor of Journal of Modern Power Systems and Clean Energy.

**Nanpeng Yu** (M'11-SM'16) received the M.S. and Ph.D. degree in electrical engineering from Iowa State University, Ames, IA, USA in 2007 and 2010 respectively. He was a Senior Power System Planner and Project Manager at Southern California Edison, Rosemead, CA, USA, from 2011 to 2014. He is currently an Assistant Professor of Electrical and Computer Engineering at University of California, Riverside, CA, USA. His current research interests include electricity market design and optimization, big data analytics in power systems, and smart energy communities.

**Jie Yan** (M'09) received the B.Eng. degree in electrical engineering from Zhejiang University, Hangzhou, China, in 2005 and the M.S. degree in electrical engineering from Huazhong University of Science and Technology, Wuhan, China, in 2007. Jie Yan received his Ph.D. degree from Iowa State University in 2011. He is currently an Senior Engineer in FTR and Pricing Administration Group in MISO, Carmel, IN 46032, USA.

**Shunbo Lei** (S'14) received the B.E. degree from Huazhong University of Science and Technology, Wuhan, China, in 2013. He is currently pursuing the Ph.D. degree with The University of Hong Kong, Hong Kong. He is currently visiting Argonne National Laboratory, Argonne, IL, USA. His research interests include operation optimization, environmental dispatch, resilience, and renewables integration of power systems.

**Weisheng Wang** (M'09-SM'15) received his Doctor degree in Electrical Engineering at Xi'an Jiaotong University in 1996. Then, he joined China Electric Power Research Institute (CEPRI) in Jan. 1997. Now, He is the director of Renewable Energy Department of CEPRI. His main interests include research and consulting in the field of renewable energy generation and its grid integration.